Proceedings of the 5th International Workshop on Hydrogen and Fuel Cells
October 26 –29, 2010
Campinas, SP, Brazil
ISSN 2179-5029

ADVANCES IN PEM FUEL CELLS WITH CFD TECHNIQUES

ERIC ROBALINHO [1]
EDGAR FERRARI DA CUNHA [1]
ZAKARYA AHMED [1],[2]
EFRAIM CEKINSKI [3]
MARCELO LINARDI [1]

[1] Instituto de Pesquisas Energéticas e Nucleares – IPEN/CNEN-SP, São Paulo, Brasil
[2] Centre National de Recherches en Sciences des Materiaux
Technopole Borj Cedria, Hammam-Lif, Tunisia
[3] Instituto de Pesquisas Tecnológicas – IPT-SP, São Paulo, Brasil

ABSTRACT
This paper presents some applications of computational fluid dynamics techniques in the optimization of Proton Exchange Membrane Fuel Cell (PEMFC) designs. The results concern: modeling of gas distribution channels, the study for both porous anode and cathode and the three-dimensional modeling of a partial geometry layer containing catalytic Gas Diffusion Layers (GDL) and membrane. Numerical results of the simulations of graphite plates flow channels, using ethanol as fuel, are also presented. Some experimental results are compared to the corresponding numerical ones for several cases, demonstrating the importance and usefulness of this computational tool.

KEY WORDS
Modeling; PEM Fuel Cell; Computational Fluid Dynamic; Numerical Analysis

1. INTRODUCTION
Nowadays, the need to obtain clean and abundant energy is one of the most concerns of the energy and materials researches. Fuel cell becomes a promising candidate to obtain this energy from renewable resources, having high power density capability and offering low to zero environmental impact. In this scenery, Proton Exchange Membrane Fuel Cell (PEMFC) is a very promising device, since it converts chemical energy directly into electrical energy and heat [1].

In general PEMFC works at low temperature (60 - 80 ℃) with high power density. These properties are ideal for portable applications, such as cell phones and computers; stationary applications, like houses, hospitals or buildings and mobile applications, cars and busses, for example [2, 3, 4]. Fuel cell simulation can provide a convenient and economic alternative for testing the fuel cells subsystems such as graphite plates or gas diffusion layers and permits also the evaluation of effects of the different fuel cells parameters (e.g. temperature, pressure, type of fuel), separately.

The search for reliable computational models is a challenge because it involves several transport phenomena: multi-component, multi-phase and multi-dimensional flow processes, electrochemical reactions, convective heat and mass transport in flow channels, diffusion of reactants through porous electrodes, transport of water through the membrane and transport of

[1] Correspondence should be addressed to Eric Robalinho:
Phone: +55 (11) 3133-9376; e-mail: eric@ipen.br

ISSN 2179-5029

electrons through solid matrix. The Computational Fluid Dynamic (CFD) is a very useful tool to simulate fuel and oxygen flow channels configurations, reducing the costs of new projects and optimizing existing market [5, 6].

Mathematical modeling is a very important part of the actual research and development work in science and engineering. In fact competitive research requires speed on path between idea and prototype, and mathematical modeling and simulation provides a valuable shortcut for understanding qualitative and quantitative aspects of scientific design.

2. OBJECTIVES

The aim of this paper is to present CFD simulations applied to fuel cell technology, showing the methodology used and some practical results comparisons.

3. MATHEMATICAL MODEL

The main hypotheses used in the modeling presented in this paper were:

- Ideal gas;
- Steady state, laminar and incompressible flux;
- Non-isothermal T = 348 K (75 ºC);
- Reactions defined as Boundary Conditions;
- Zero external forces;
- Isotropic and homogeneous materials;
- Thermodynamic and electrochemical properties are constants;
- Mono-phase.

The domains of calculus are the first and most important step, when one wants to model some physical phenomena. Domains of computation are partial or global, depending on the results needed. The 3D domains Entire Plate Model and MEA Model are two models used often in simulations [7] as can be seen in Figure 1.

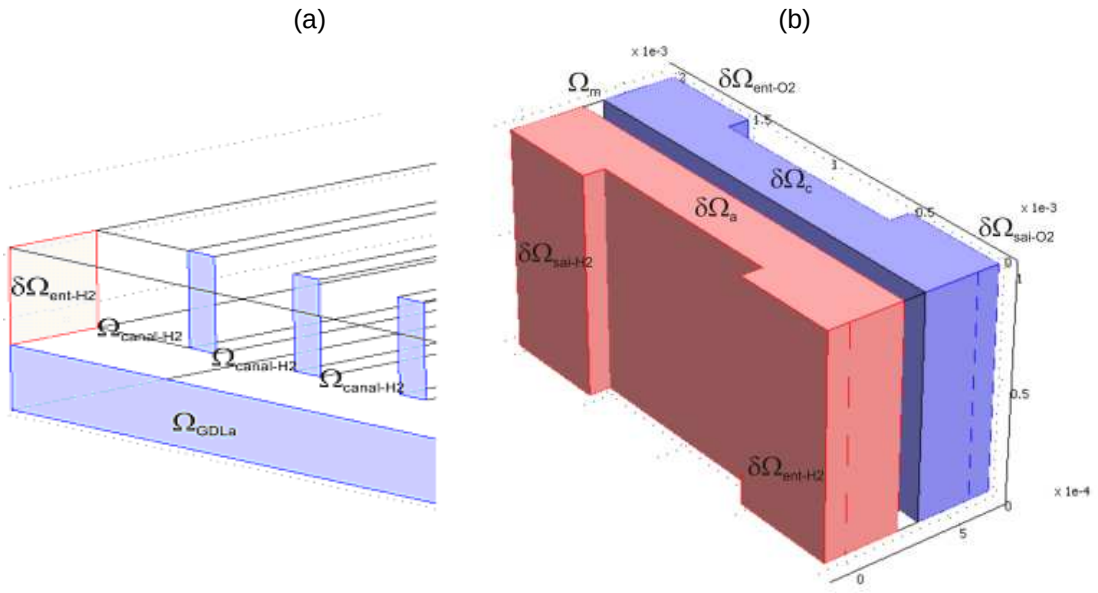

Figure 1: (a) Entire Plate Model and (b) MEA Model [7].

To solve computationally the proposed problem, robust hardware and software are necessary. In these cases Intel 5320 Quad Core XEON Workstation were used, 16GB RAM and COMSOL Multiphysics program version 3.3a.

The evaluation of the cell potential was determined as:

$$E = E_0 - V_{ativ} - V_{resist} - V_{conc}$$

or,

$$E = E_0 - (V_{ativ} + V_{conc})_a - (V_{ativ} + V_{conc})_c - V_{resist}$$

The cell potential was obtained by Nernst equation [8]:

$$E = -\frac{\Delta G}{nF} = E_{0,c} - E_{0,a} = E_0 + \frac{RT}{nF}\ln\left[\frac{p_{H2}p_{O2}^{\ 0,5}}{p_{H2O}}\right]$$

For example,

$H_2 + 1/2\ O_2 \rightarrow H_2O_{(l)}$ $\Delta G = -237{,}3$ kJ/mol, $E_0 = 1{,}23$ V

The gas distribution channels were modeled by Navier-Stokes and continuity equations:

$$\rho\frac{\partial u}{\partial t} - \nabla\eta(\nabla u + [\nabla u]^t) + \rho(u.\nabla)u + \nabla p = 0$$

$$\nabla.u = 0$$

The GDL layer was represented by Brinkman and continuity equations:

$$\rho\frac{\partial u}{\partial t} - \eta\Delta u + \frac{\eta}{kp}u + \nabla p = 0$$

$$\nabla.u = 0$$

The catalytic layer was represented by Agglomerated Model geometry and it was modeled through the Butler-Volmer equation [9]:

$$i = i_0\left\{\exp\left[\frac{-\alpha_R F(E-E_0)}{RT}\right] - \exp\left[\frac{\alpha_O F(E-E_0)}{RT}\right]\right\}$$

The current density of anode and cathode were given considering the last formulation and data from experimental and literature source, respectively by [10, 11]:

$$i_a = -6\,l_{cat}\,(1-e\_mac)\,F\left[\frac{D_{ag}}{R_{ag}^2}\right]\left[1 - R_{ag}\sqrt{\frac{i_{0,a}Sa}{2Fc_{H2}^{ref}D_{ag}}}\coth\left(R_{ag}\sqrt{\frac{i_{0,a}Sa}{2Fc_{H2}^{ref}D_{ag}}}\right)\right]\left[c_{H2}^{ag} - c_{H2}^{ref}\exp\left(\frac{-F}{RT}\eta_P\right)\right]$$

and

$$i_c = 12\,l_{cat}\,(1-e\_mac)\,F\left[\frac{D_{ag}}{R_{ag}^2}\right]\left[1 - \sqrt{\frac{i_{0,c}SaR_{ag}^2}{4Fc_{O2}^{ref}D_{ag}}\exp\left(\frac{2F}{RT}\eta_P\right)}\coth\sqrt{\frac{i_{0,c}SaR_{ag}^2}{4Fc_{O2}^{ref}D_{ag}}\exp\left(\frac{2F}{RT}\eta_P\right)}\right]\left[c_{O2}^{ag}\right]$$

The mass balance was performed dynamically by Maxwell-Stefan approach:

ISSN 2179-5029

$$\frac{\partial}{\partial t}\rho\omega_i + \nabla.\left[-\rho\omega_i\sum_{j=1}^{N} D_{ij}\left\{\frac{M}{M_j}\left(\nabla\omega_j + \omega_j\frac{\nabla M}{M}\right) + \left(x_j - \omega_j\right)\frac{\nabla p}{p}\right\} + \omega_i\rho\mathbf{u} + D_i^T\frac{\nabla T}{T}\right] = \Re_i$$

The charge balance was calculated by Laplace equation:

$$\nabla.[-k\nabla\phi] = 0$$

The coupling of the models was done via pressure values, obtained by Entire Plate Model, and used as initial conditions for the implementation of the equations of Darcy. Thus, determining the velocity vectors for mass balance (Maxwell-Stefan equations), the MEA Model calculates the distribution of current densities related on given potential distribution [7].

The PEMFC consists of two main parts. The first one is an electrolyte between two Gas Diffusion Electrodes (GDE), an anode and a cathode with two Gas Diffusion Layers (GDL). This structure is called Membrane Electrode Assembly (MEA). The second part is the gas flow field plates, called bipolar plates, in the case of a stack. The experimental part uses single cells and systems with more than one set of membrane – carbon plates (stack), as showed in Figure 2.

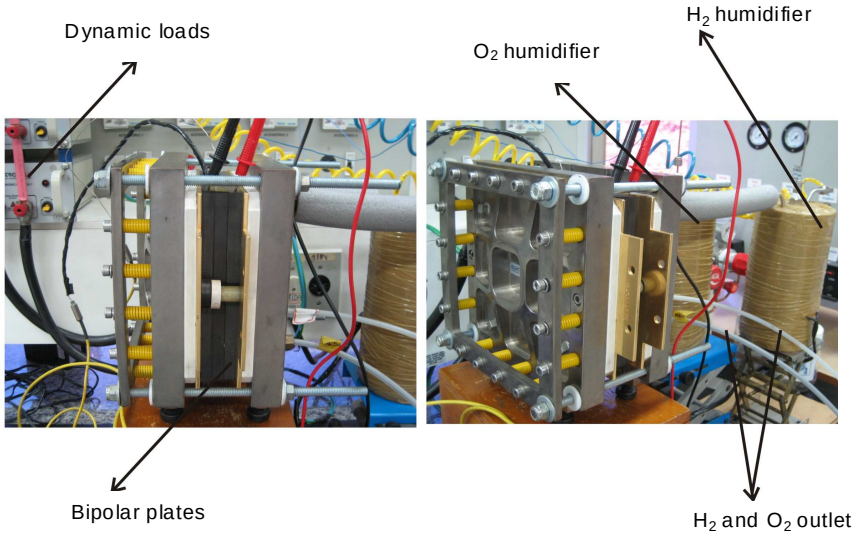

Figure 2: PEMFC setup [7].

4. Results and Discussion

4.1 Case 1: Development of Bipolar Plates

Two 144 cm² of geometric area single cells were manufactured and used (prototypes1 and 2). The serpentine/parallel flow field for channel geometry was chosen. The configurations of flow field in the prototype 1 were: width: 2.0 mm; depth: 2.0 mm; and ribs: 2.0 mm. For prototype 2: width: 1.5 mm; depth: 1.5 mm; and ribs: 0.5 mm [12, 13, 14]. In Figure 3 the both bipolar plates are showed.

(a) (b)

ISSN 2179-5029

Figure 3: Flow field channels from (a) prototype 1 and (b) prototype 2.

The velocity magnitude throughout the field channels was studied to design the channels and simulate 2D velocity profiles. In Figure 4 details of the simulations for the gas entrance and some channels in prototype 1 (a) and prototype 2 (b) are showed.

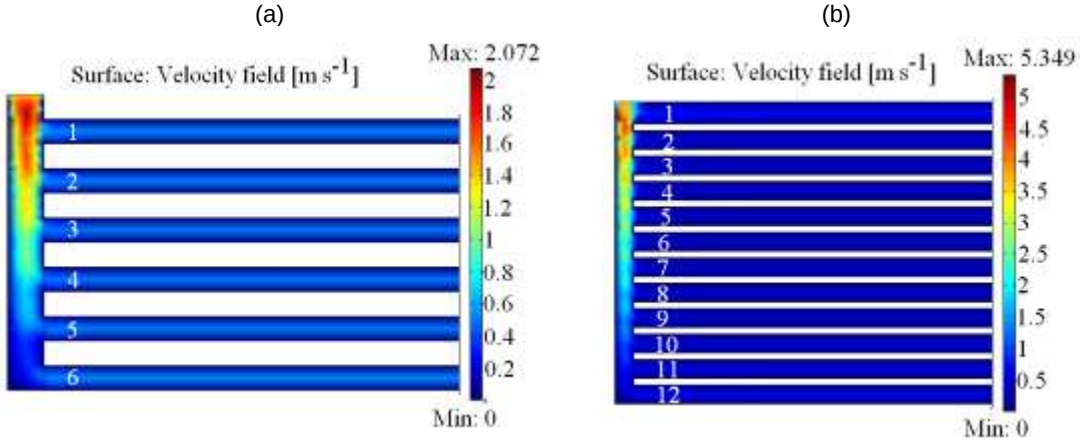

Figure 4: Velocity flow fields for (a) prototype 1 and (b) prototype 2 [13].

In Figure 5 the velocity profiles in the middle of the first set of the serpentine path for (a) prototype 1 and (b) for prototype 2 are showed. Each channel is represented by one peek.

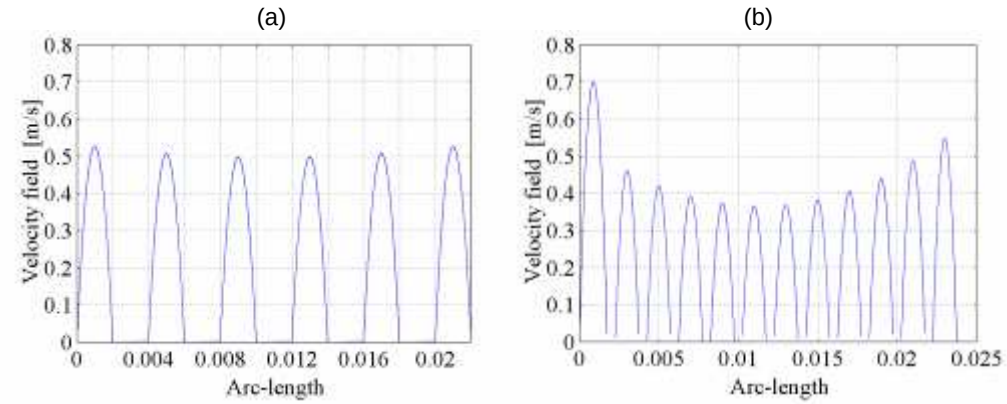

Figure 5: Velocity profile in each channel for (a) prototype 1 and (b) prototype 2 [13].

For prototypes 1 and 2, a study of their partial geometries consisting of the inlet and two channels with the porous media was carried out. For this, two graphite plates were simulated to

ISSN 2179-5029

investigate the hydrogen flow, pressure drops. Implementations of the modeling allowed the optimization the design of the plates and better understanding the fuel cell dynamics.

The Nonlinear solver for stationary analysis was set by COMSOL Multiphysics automatically, and the Spooles direct solver was selected for linear conditions. The Spooles uses the multifrontal method and direct LU factorization of the sparse matrix A to solve systems of the form Ax=b. There are several solver methods available, including the iterative ones that are less stable than direct solvers and they do not always converge.

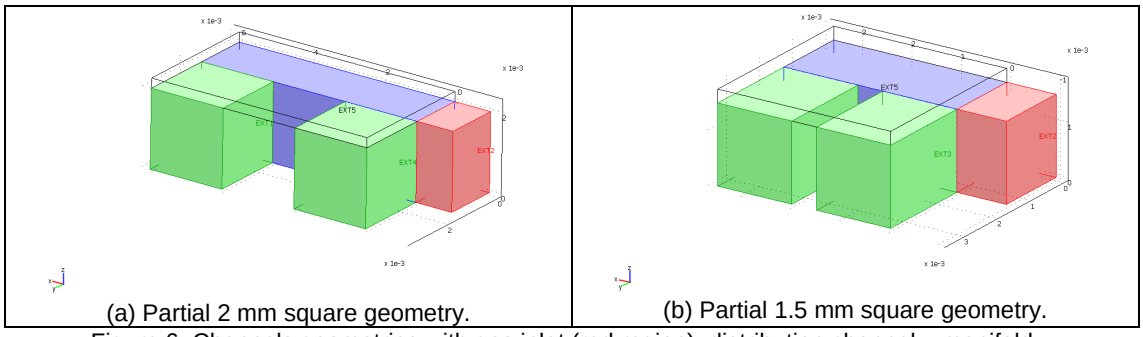

(a) Partial 2 mm square geometry. (b) Partial 1.5 mm square geometry.

Figure 6: Channels geometries with gas inlet (red region); distribution channel – manifold – (blue region); and two channels (green region) [14].

In Figure 6 the chosen channels geometries are showed. The red region represents the gas inlet, the blue one is the distribution place and the green is the initial part of two channels. The area above the channels (0.25 mm thickness transparent rectangle) represents the GDL.

In the Table 1 the different meshes and corresponding solutions time were compared. The convergence in these cases was obtained in 3 to 7 iterations and the relative tolerance at nonlinear solver was set on 10^{-6}. The refinement method was set on longest, with the best quality option. The mesh in each simulation was defined by the Number of Degrees of Freedom (NOF'S), the Number of Elements (NE) and the Minimum Element Quality (MEQ). As can be seen in Table 1, the increasing of mesh refinement required much more solution time and availability of memory.

Table 1: Different meshes and corresponding NOF'S, NE, MEQ and SOLUTION TIME [14].

	MESH	NOF'S	NE	MEQ	SOLUTION TIME (s)
SQUARE (2 mm)	Coarser	6729	769	0.3080	9.2
	Coarse	10425	1273	0.2944	17.7
	Normal	19148	2563	0.3498	56.2
	Fine	29260	4144	0.3696	149.8
	Finer	83845	12718	0.3422	1891.2
SQUARE (1.5 mm)	Coarser	7496	937	0.3230	12.7
	Coarse	14962	1867	0.2823	42.3
	Normal	31808	4509	0.3195	241.5
	Fine	56461	8369	0.3868	908.5
	Finer	158145	24959	0.2715	17592.2

The model uses normal/pressure boundary conditions for inlet and convective flux for outlet. The condition for porosity (porous media) was found in Navier-Stokes module in COMSOL Multiphysics, which was set on 10^{-12} m^2 for permeability of GDL.

Pressure lines graphics were plotted for each profile studied. For one predetermined channel length, y =3.50 mm, six pressure lines were plotted at the GDL interior and one at the channel outlet (0.05 mm from the upper surface of the channel), in order to evaluate the pressure gradient there [15]. The pressure gradient behavior of the studied models provides homogeneity of the reactants gas flux data through diffusion layer. A homogeneous pressure gradient means higher gas availability for the fuel cell reactions.

ISSN 2179-5029

According to the graphics shown, a huge stagnation region (dead zone) is noticed at the top of rib between the 2 mm square profile channels. In Figure 7 this effect is noticed from the inexistence of a high pressure gradient at 2.50 mm < x < 3.50 mm range (every pressure lines were close to zero). The 1.5 square profile presents stagnation, but it is local surrounding x=1.75 mm (Figure 8). The trapezoidal and triangular profile channels presented similar responses about pressure gradient throughout the geometry, with no stagnation zones.

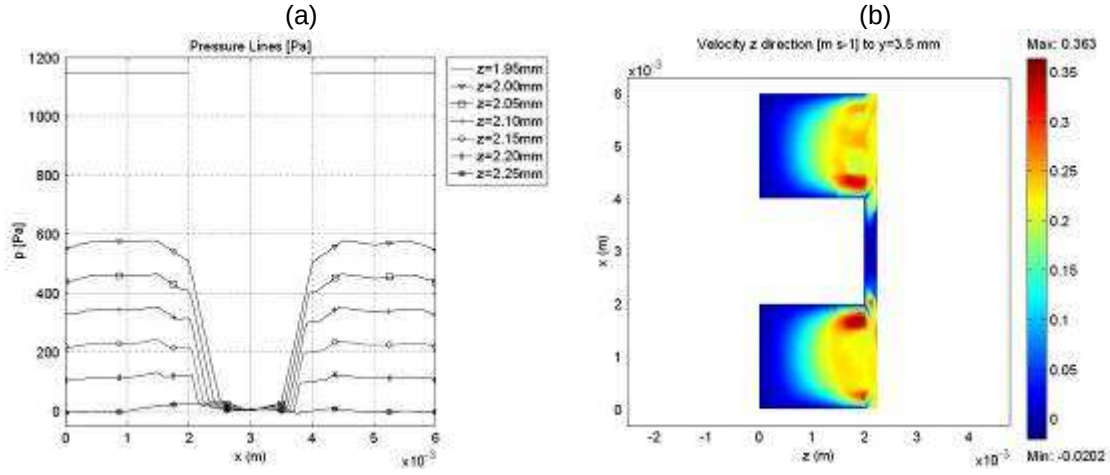

Figure 7: (a) Pressure lines and (b) z-velocity slice of 2 mm square profile [15].

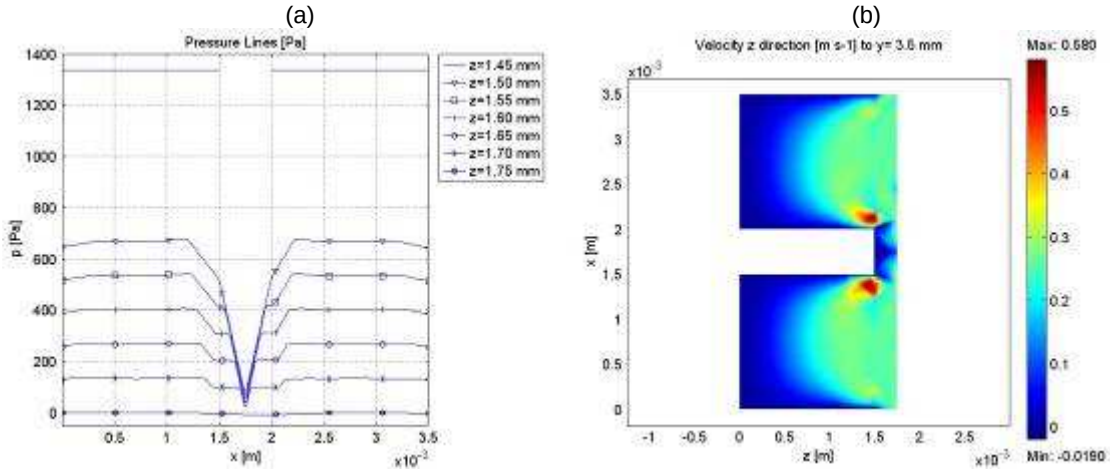

Figure 8: (a) Pressure lines and (b) z-velocity slice of 1.5 mm square profile [15].

In the Figures 7 and 8 the z-velocity slice profiles for all channels configurations are showed. At velocity slice graphic (Figure 8) of 2 mm square profile, there was a remarkable region of low velocity in z, confirming the obtained results by pressure lines. The square profiles presented areas or spots of large decreasing velocity (hitting 0.1 m s^{-1} at diffusion layer outlet, z = 2.25 mm at 2 mm square profile and z = 1.75 mm at 1.5 mm square profile).

In order to check the studied models correspondence within actual fuel cell experiments, both square profiles (graphite plates) were used. The polarization curve measures the fuel cell performance in terms of potential drop, under different values of current. The value of 0.6V (work potential) was set to compare two different fuel cells performance. In Figure 9 the polarization curves of the both prototypes were presented. The values for work operation were: 166.7 mA cm^{-2} and 470.6 mA cm^{-2}, for the prototype 1 and 2, respectively. The graphite plate in

ISSN 2179-5029

prototype 2 had better performance than in the prototype 1, which was validated by numeric methods. Such behavior was attributed to the high channel area in contact with gas diffusion electrode that provides higher active area available for the gas reaction. Besides the area, increasing gas velocities in flow fields decrease the gas stagnation points along the channels.

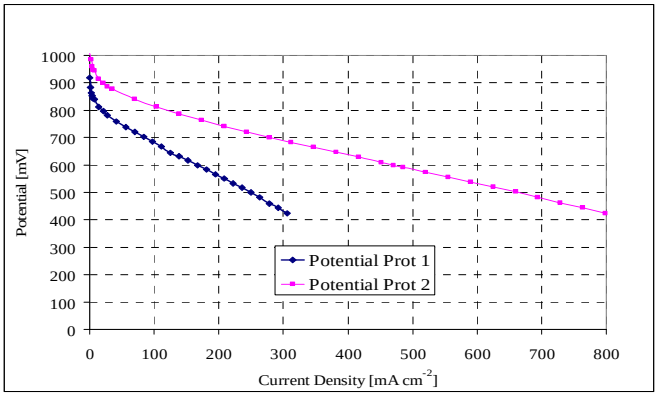

Figure 9: Polarization curves of prototype 1 and prototype 2 [15].

Several models of simulations for diffusion in porous media and conduction/convection processes were studied. Then, the experimental data were used to visualize the differences in performance between prototypes 1 and 2. The graphite plate in prototype 2 exhibited better performance than in prototype 1, which was validated by numeric methods. Such behavior was attributed to the high channel area in contact with gas diffusion electrode, which provides high active area available for the gas reaction. Besides the area, increasing gas velocities in flow fields decrease the number of gas stagnation points along the channels.

Other two geometries were studied: triangular and trapezoidal ribs. For these two cases, experimental part was not realized yet. For this reason, these simulations were not presented and these geometries are under studies.

The CFD techniques are a research tool to explore the connection between the transport of reactants and products and overall cell performance. CFD simulates hydrogen gas flow channels to reduce the costs of bipolar plates production through optimization of the mass transport.

4.2 Case 2: Development of a Numerical Model applied to unit PEMFC

In this case, the development of a numerical model to study unit PEM cells with geometric area of 144 cm^2 on a macroscopic scale was carried out. Besides that, the study contemplated the production and operation of a prototype of a PEM fuel cell with its respective bipolar plate. The analyses of the numerical results were performed and some of the post-processing data were showed in this paper [7]. The studies of most important parameters were performed, as well as the numerical study of operating temperatures of the cell and the dependence of the mesh for 3D models [16, 17, 18, 19, 20, 21].

In all experiments, the polarization and power density curves for steady state were obtained using the TDI Dynaload Electronic Load Model RBL 488-50-150-800. All fuel cells were operated using pure hydrogen, saturated with water vapor at 85 ºC and pure oxygen, also saturated with water vapor at 70 ºC, at atmospheric pressure. The fuel cells were maintained at constant temperature of 75 ºC using thermostats.

The distribution of ionic current densities is showed in Figure 10, where there is a non-uniform distribution of the measured quantity. The distributions of mass fractions of H_2 and O_2, and also of H_2O are showed in Figure 11.

ISSN 2179-5029

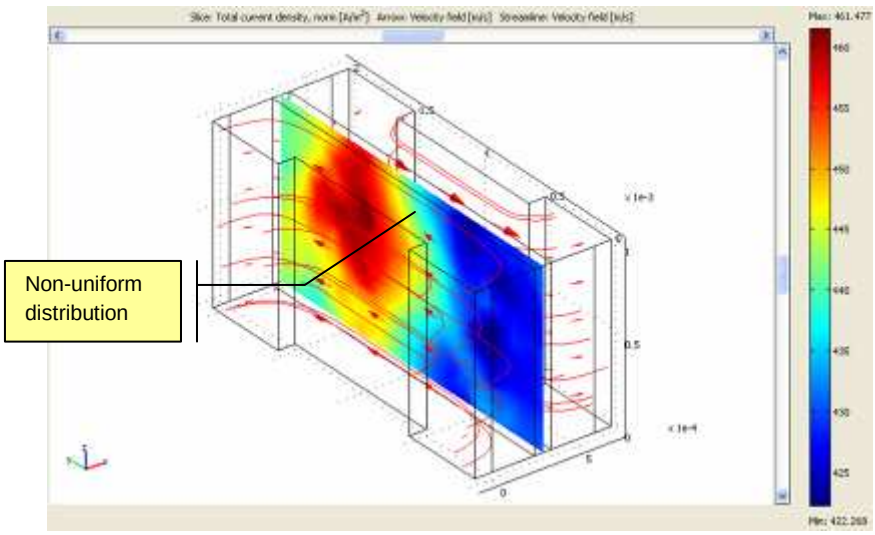

Figure 10: YZ section, distribution of ionic current densities in the median plane of the membrane. Operating conditions: T_{cel}=75 ºC, p_{ref}=1 atm, pH_2=pO_2=52.45 Pa, V_{cel}=0.7 V [7].

In Figure 12 the variation of mass fraction (to H_2 and O_2) can be observed as isosurfaces in a 3D post-processing of COMSOL Multiphysics.

The Figure 13 shows the polarizations curves for experimental data. In order to compare the results, Figure 14 shows the approximation to MEA 02, that demonstrates a good correlation between them.

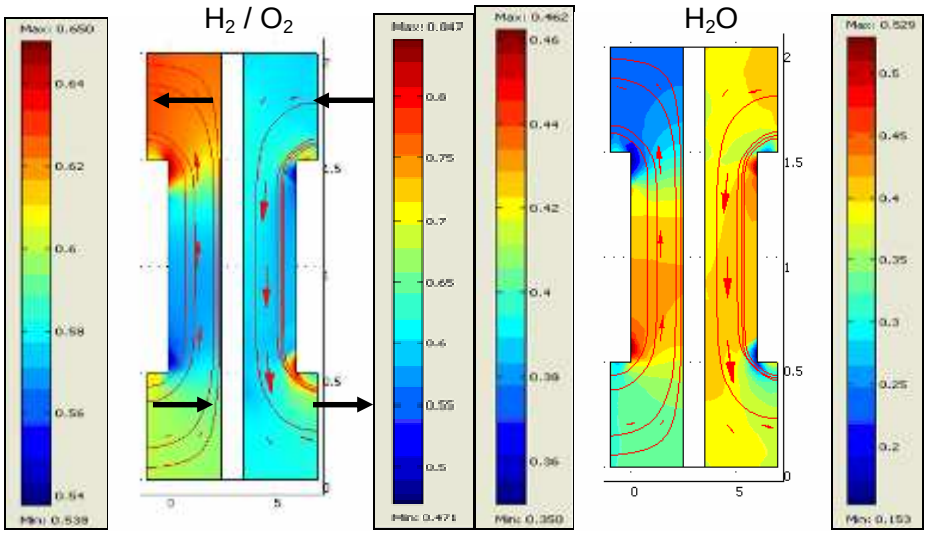

Figure 11: XY section, distributions of mass fractions of H_2 and O_2, and H_2O. Operating conditions: T_{cel}=75 ºC, p_{ref}=1 atm, pH_2=pO_2=52.45 Pa, V_{cel}=0.7 V [7].

ISSN 2179-5029

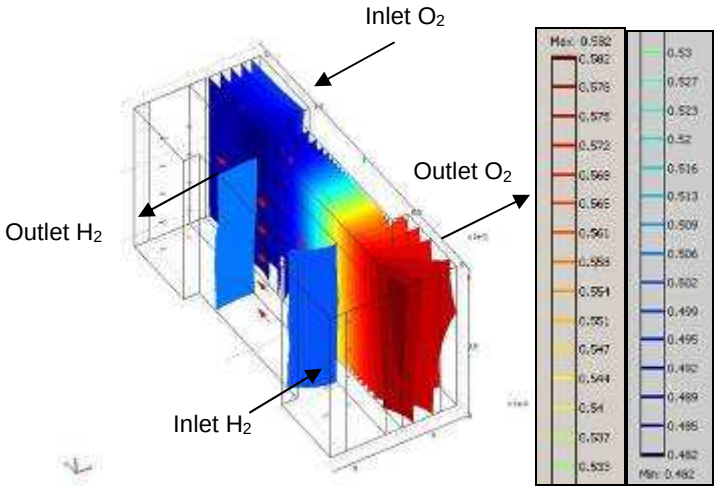

Figure 12: Isosurfaces for mass fractions ωH_2 and ωO_2, for the basecase.
Operating conditions: T_{cel}=75 ºC, p_{ref}=1 atm, pH_2=pO_2=52.45 Pa [7].

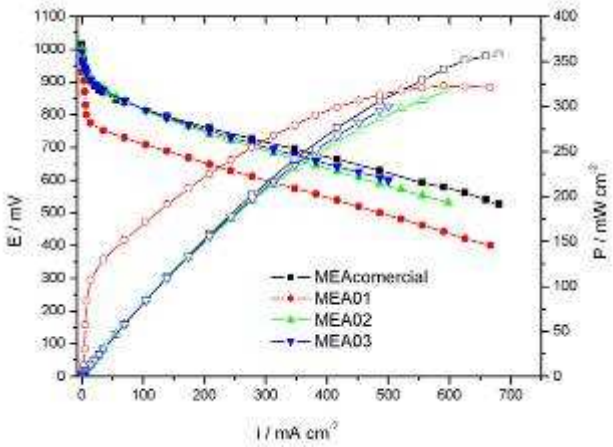

Figure 13: Experimental results (MEAs 01, 02, 03) versus commercial.
Operating conditions: T_{cel}= 75 ºC, $T_{u,a}$=85 ºC, $T_{u,c}$=70 ºC, p_{ref}=1 atm, H_2/O_2, flow: 2 x stoichiometric [7].

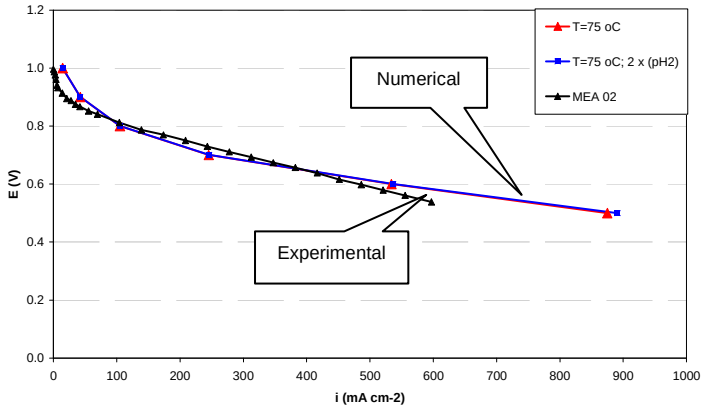

Figure 14: Numerical X experimental results for MEA 02. Operating conditions:
T_{cel}= 75 ºC, $T_{u,a}$=85 ºC, $T_{u,c}$=70 ºC, P=1 atm, H_2/O_2, flow: 2 x stoichiometric.
Numerical results: T_{cel}=75 ºC, p_{ref}=1 atm, p_{H2}=p_{O2}=20.0 Pa [7].

ISSN 2179-5029

The polarization curves are representations of the performance of each membrane-electrode assembly (MEA). Besides the potential X current density curves, one can obtain other information about the fuel cell in operation, for example, the power densities curve (mW cm^{-2}). This potential is chosen according to the application of the fuel cell [8]. A fuel cell that has large area (as studied here) may be more efficient than a compact cell, since they select adequately the potential of operation. The MEA 02 has current density of approximately 480 mA cm^{-2} for the operating potential of 0.6 V. Selecting a lower potential (e.g. 0.5 V), means getting a lower efficiency and higher current densities.

The polarization curves in Figure 14 show the consistent results, regarding the comparison between the measurements for initial case (75 ℃) and the same simulation with double stoichiometric values of anode pressure. There are no significant differences for these curves, since they are coincident. Regarding the experimental curve MEA 02, there is a reasonable fit, considering that the possibility of refinements in some values of variables used in the numerical model (e.g. pressure, mass fractions and porosities). For the high potential range, activation overpotentials, respective numerical values are just above (maximum 5%) with relation to the values obtained in the laboratory. This behavior is also noted for values above 600 mA cm^{-2} current density, which means that the curve does not present perfect numerical fit in the regions of mass transport. In the middle range, where one observes the actual real operating conditions, there is quite satisfactory agreement (with error less than 5%) between experimental and numerical values.

The adjustment of the numerical curve in the region of activation polarization indicates a more refined determination of the numeric value of exchange current density. For the value reported in the literature used in the modeling developed in this work, the approach shown in Figure 14 was the best result [7].

4.3 Case 3: Study of Direct Ethanol Fuel Cell (DEFC)

This is a preliminary study of use of different fuel then hydrogen (ethanol, in this case) [22, 23]. A single cell of 5 cm^2 was used for the DEFC experiment. Figure 15 shows the experimental polarization curves of fuel cells using Nafion membrane, operating at 80 ℃ fed with ethanol solution (2 mol L^{-1}) at flow rates of 2 mL min^{-1} and 4 mL min^{-1} in the anode, and pure oxygen in the cathode.

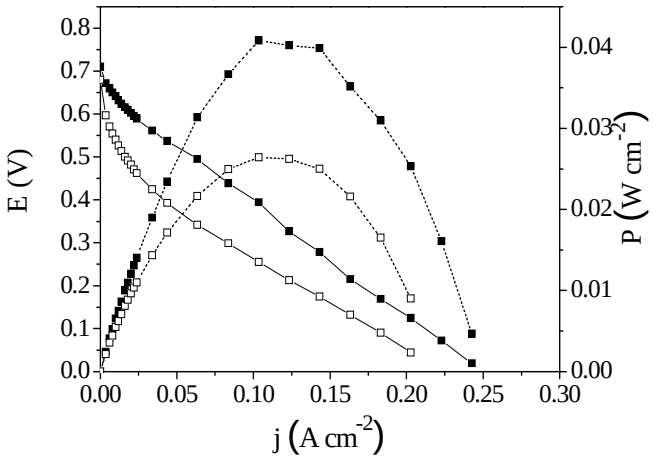

Figure 15: Experimental polarization curves of direct ethanol fuel cells using Nafion membrane (80 ℃) [24].

The first step of modeling of this system was chosen, to start with the study of temperature, velocity and pressure distribution. The complete modeling of the fuel cells (including electrochemical reactions) is yet under investigation.

ISSN 2179-5029

The geometric domain and the mesh (239916 elements) for the transient analysis of the temperature distribution is showed below. In Figure 16 the half cell containing the two cartridges heaters in the aluminum plate and one graphite plate can be observed.

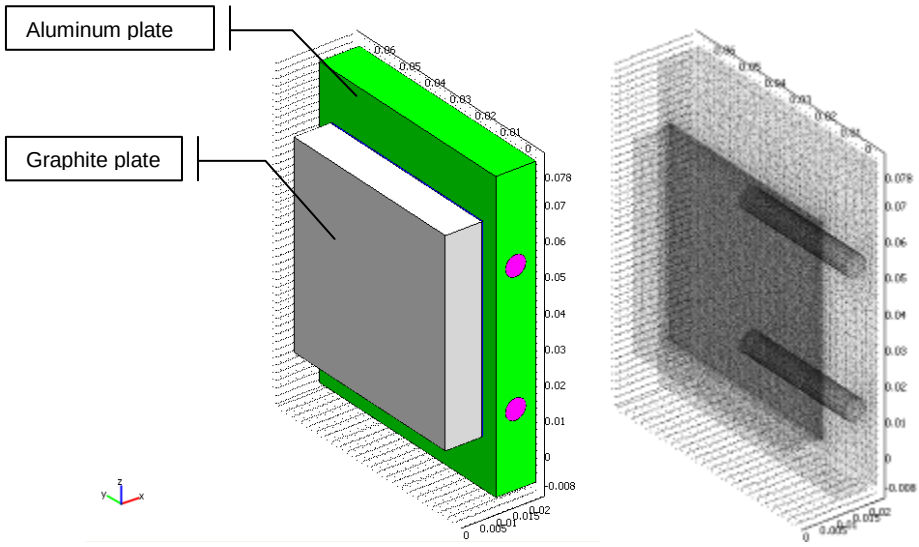

Figure 16: Geometric domain and mesh for the transient analysis of temperature.

The results of this simulation are showed in the Figure 17. These simulations were used to identify the heat conductive process that occurs in the different materials in the fuel cell. The gradients of temperature were observed and the heaters and plates chosen were satisfactory.

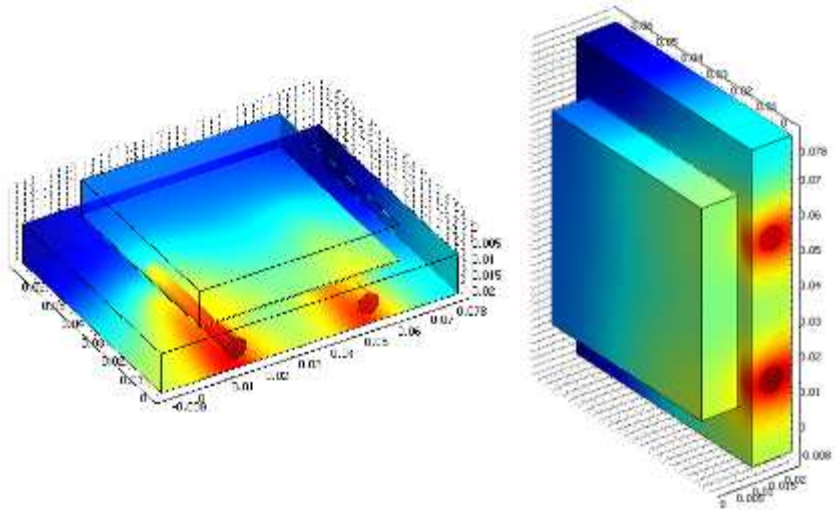

Figure 17: Result for the transient analysis of temperature.

Figure 18 shows velocity and pressure distribution for system using pure ethanol. The values of pressure and velocity distributions refer to measurements obtained in the distribution channels - GDL interface.

ISSN 2179-5029

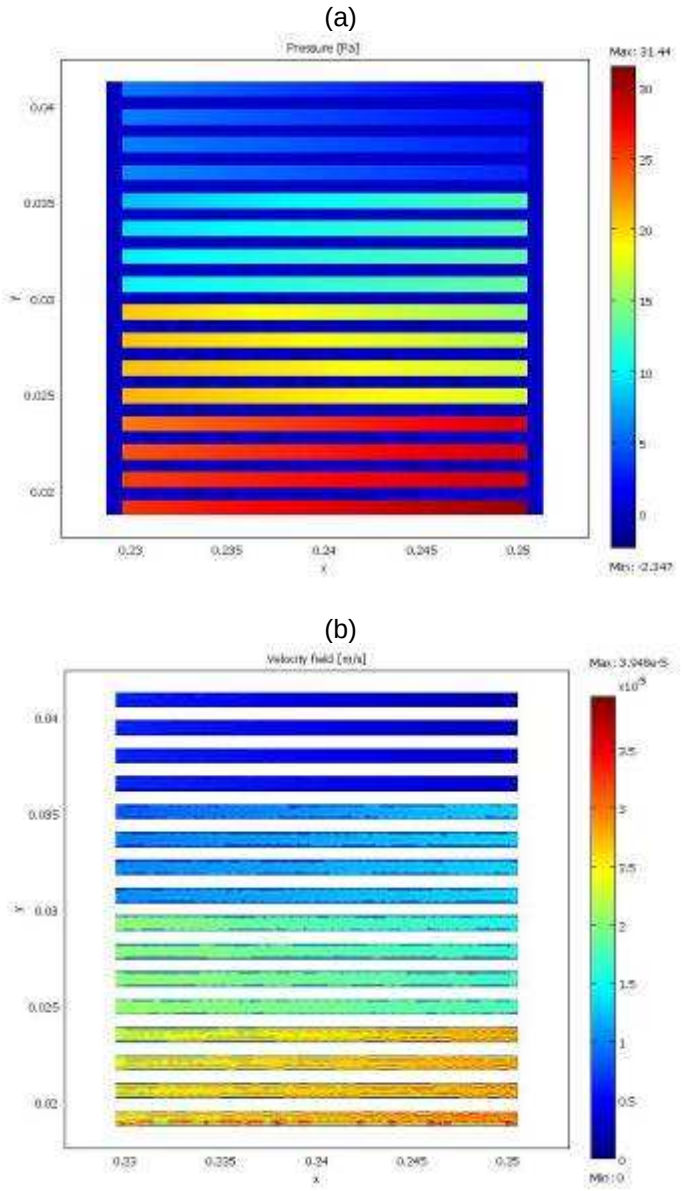

Figure 18: (a) Pressure and (b) velocity distribution results for system using ethanol as fuel.

Comparing to a hydrogen gas flow (not showed data), in the same simulation conditions, the pressure drop was much lower than the one in case of ethanol flow. Otherwise, the maximum velocity flux with hydrogen was quite similar to ethanol.

5. CONCLUSIONS

The modeling process developed in this work presents itself as an additional useful tool for developing new projects for fuel cells. The modeling helps the designer in the choice of materials, geometric configurations and structures for manufacturing and testing. Tests have resulted in final prototypes or improvements of existing projects. In this sense, such diagnoses were of great importance not only to identify design errors, but also to adjust and propose improvements in fuel cell systems already in operation. The proposed model is robust and able to provide quick responses and is also very helpful, predicting satisfactorily the cell performance over a wide range of operating conditions. The use of CFD tool make possible to develop

further work on applications of high temperature PEM even using other fuels such as ethanol or methanol.

6. ACKNOWLEDGEMENTS

This work was supported by CNPq and IPEN/CNEN-SP Laboratories.

7. REFERENCES

[1] LINARDI, MARCELO **Introdução à Ciência e Tecnologia de Células a Combustível**, São Paulo: Artliber, 2010.

[2] AKBARI, M.H. **PEM Fuel Cell Systems for Electric Power Generation**: An Overview, Proceedings International Hydrogen Energy Congress and Exhibition IHEC 2005. Istanbul, Turkey, 13-15 July 2005.

[3] ZHANG, JIUJUN. **PEM Fuel Cell Electrocatalysts and Catalyst Layers**: Fundamentals and Applications, Springer-Verlag London Limited, 2008.

[4] SILVA, A.C.; ROBALINHO, E. **Desenvolvimento Tecnológico e Oportunidades de Aplicação de Células a Combustível no segmento de backup de energia.** Especialização em Gestão Estratégica de Tecnologia – MBA, Instituto de Pesquisas Tecnológicas do Estado de São Paulo – IPT, São Paulo, 2007.

[5] **Fuel Cell Handbook**, 7.ed., EG&G Technical Services, Inc., U.S.Department of Energy – USDOE, Office of Fossil Energy, National Energy Technology Laboratory, Morgantown, West Virginia, USA, November 2004.

[6] LARMINIE, J.; DICKS, A. **Fuel Cell Systems Explained**. 2.ed. Chichester: John Wiley & Sons, England, 2003.

[7] ROBALINHO, E. **Desenvolvimento de um modelo numérico computacional aplicado a uma célula a combustível de 144 cm^2 tipo PEM**. Tese de Doutorado, Instituto de Pesquisas Energéticas e Nucleares IPEN – USP, São Paulo, SP, 2009.

[8] BARBIR, FRANO. **PEM Fuel Cells – Theory and Practice**, Elsevier Academic Press, 2005.

[9] BARD, A. J. E FAULKNER, L. R. **Electrochemical Methods**. New York: John Wiley & Sons, 1980.

[10] SPRINGER, T.E; RAISTRICK, I.D. **Electrical Impedance of a Pore Wall for the Flooded-Agglomerate Model of Porous Gas-Diffusion Electrodes**. J. Eletrochem. Soc., v. 136, n. 6, p. 1594-1603, June 1989.

[11] BROKA, K. **Characterization of the Components of the Proton Exchange Membrane Fuel Cell.** Techn. Lic. Thesis, Royal Institute of Technology, Stockholm, 1995.

[12] ROBALINHO, E. **Modelagem e simulação de placas bipolares para células tipo PEMFC**. 3º. Encontro sobre Célula a Combustível, IPEN, 29 e 30 de novembro, São Paulo, 2007.

[13] CUNHA, E. F.; ANDRADE, A. B.; ROBALINHO, E.; BEJARANO, M. L. M.; CEKINSKI, E.; LINARDI, M. **Modelling and Simulation of PEM Fuel Cell's Flow Channels using CFD Techniques**. INAC 2007, São Paulo, 2007.

[14] ROBALINHO, E.; CUNHA, E. F.; ANDRADE, A. B.; BEJARANO, M. L. M.; LINARDI, M.; CEKINSKI, E. COMSOL **Modelling and Simulation of PEM Fuel Cell's Flow Channels**. Comsol® Conference 2007, Boston, USA, 2007.

[15] CUNHA, E. F.; ROBALINHO, E.; ANDRADE, A. B.; BEJARANO, M. L. M.; CEKINSKI, E.; LINARDI, M. **Application of CFD Techniques in the Modelling and Simulation of PEM Fuel Cell´s Flow Channels**. 2nd. European Fuel Cell Technology and Applications Conference, EFC 2007.

[16] EIKERLING, MICHAEL **Physical Modeling of PEM Fuel Cells**. Fuel Cell Workshop, Brasília, April 9-13, 2007.

[17] BURDEN, R. L.; FAIRES, J. D. **Numerical Analysis**. 4.ed., PWS-Kent Pub Co., 1989.

[18] CARNES, B.; DJILALI, N. **Systematic parameter estimation for PEM fuel cell models**. Journal of Power Sources, v. 144, p. 83-93, 2005.

[19] LE, ANH DINH; ZHOU, BIAO. **A General Model of Proton Exchange Membrane Fuel Cell**. Journal of Power Sources, v. 182, p. 197-222, 2008.

[20] BERNARDI, D.M.; VERBRUGGE, M.W. **A Mathematical Model of the Solid-Polymer-Electrolyte Fuel Cell** J. Eletrochem. Soc., v. 139, n. 9, p. 2477-2490, 1992.

[21] BIRD, R. B., STEWART, W. E.; LIGHTFOOT, E. N. **Transport Phenomena**. New York: John Wiley & Sons, 1960.

[22] SONG. S.; P. TSIAKARAS, P.; **Recent progress in direct ethanol proton exchange membrane fuel cells (DE-PEMFCs).** App. Catal. B. Environ., v. 63, p. 187-193, 2006.

[23] PEIGHAMBARDOUST, S. J.; ROWSHANZAMIR, S.; AMJADI, M. **Review of the proton exchange membranes for fuel cell applications.** International J. of Hydrogen Energy, In Press, 2010.

[24] AHMED, Z.; MATOS, B. R.; FLORIO, D. Z.; LICOCCIA, S.; TRAVERSSA, E.; ESPOSITO, V.; SANTIAGO, E. I.; FONSECA, F. C. **Nafion-Mesoporous Silica as Electrolyte for Ethanol Fuel Cells.** ECS Trans., v. 25, p. 853-860, issue 1, 2009.